The FLUKA code: description and benchmarking

G. Battistoni*, F. Cerutti†, A. Fassò**, A. Ferrari†, S. Muraro*, J. Ranft‡, S. Roesler† and P.R. Sala*

*INFN sezione di Milano, via Celoria 16, I-20133 Milano, Italy
†CERN, CH-1211 GENEVE 23, Switzerland
**SLAC, Stanford, USA
‡Siegen University, Germany

Abstract. The physics model implemented inside the FLUKA code are briefly described, with emphasis on hadronic interactions. Examples of the capabilities of the code are presented including basic (thin target) and complex benchmarks.

Keywords: Monte Carlo simulations, calorimetry, nuclear interactions
PACS: 02.70.Uu; 24.10.Lx; 87.53.Wz; 29.40.Vj

INTRODUCTION

The FLUKA code [1] is a general purpose Monte Carlo code for the interaction and transport of hadrons, heavy ions, and electromagnetic particles from few keV (or thermal energies for neutrons) to cosmic ray energies in whichever material. It is built and maintained with the aim of including the best possible physical models in terms of completeness and precision. In this "microscopic" approach, each step has sound physical basis. Performances are optimized comparing with particle production data at single interaction level. No tuning whatsoever on "integral" data, like calorimeter resolutions, thick target yields etc, is performed. Therefore, final predictions are obtained with minimal free parameters, fixed for all energies and target/projectile combinations. Results in complex cases as well as scaling laws and properties come out naturally from the underlying physical models and the basic conservation laws are fulfilled "a priori". Moreover, the microscopic approach preserves correlations within interactions and among the shower components, and it provides predictions where no experimental data is directly available.

When needed, powerful biasing techniques are available to reduce computing time.

Descriptions of FLUKA models and extensive benchmarking can be found in the literature (see the web page, `www.fluka.org`). The development and maintenance of FLUKA are performed in the framework of an INFN–CERN agreement.

Old versions of the FLUKA hadronic models are still used by other codes. The 1993 version of the FLUKA hadronic physics [2], excluding the intermediate energy model, was interfaced to GEANT3 [3], and activated both by the so-called GEANT-FLUKA package at all energies, and by the GEANT-CALOR package for interactions above 5-10 GeV. The 1990 version has been made available to LAHET [4] and MCNPX [5] users. No upgrade of these interfaces has been performed and they have to be considered

31

obsolete; their results are not representative of the present performances of the FLUKA hadronic models. The CORSIKA simulation package [6] also includes the FLUKA hadronic routines as an option [7], but in this case the interface is kept up to date.

E.M. and muon transport in FLUKA

For historical reasons, FLUKA is best known for its hadron event generators, but since more than 17 years FLUKA can handle with similar or better accuracy electromagnetic effects [8]. Briefly, the energy range covered by this sector of FLUKA is very wide: the program can transport photons and electrons over about 12 energy decades, from 1 PeV down to 1 keV. The e.m. part is fully coupled with the hadron sector, including the low energy (i.e. < 20 MeV) neutrons. The simulation of the electromagnetic cascade in FLUKA is very accurate, including the Landau-Pomeranchuk-Migdal effect and a special treatment of the tip of the bremsstrahlung spectrum. Electron pairs and bremsstrahlung are sampled from the proper double differential energy-angular distributions improving the common practice of using average angles. In a similar way, the three-dimensional shape of the e.m. cascades is reproduced in detail by a rigorous sampling of correlated energy and angles in decay, scattering, and multiple Coulomb scattering.

Recently, since the FLUKA2005.6 version, the need for an external cross section preprocessor has been eliminated, integrating all the needed functionality into the initialization stage. At the same time, data from the EPDL97 [9] photon cross section library have become the source for pair production, photoelectric and total coherent cross-section tabulations, as well as for atomic form factor data.

Bremsstrahlung and direct pair production by muons are modeled according to state-of-the-art theoretical description and have been checked against experimental data [10, 11]. Muon photonuclear interactions are also modeled.

CHARGED PARTICLE TRANSPORT

Transport of charged particles is performed through an original Multiple Coulomb scattering algorithm [12], supplemented by an optional single scattering method. The treatment of ionization energy loss is based on a statistical approach alternative to the standard Landau and Vavilov ones that provides a very good reproduction of average ionization and of fluctuations [13]. Multiple scattering with inclusion of nuclear form factors is applied also to heavy ion transport. Up-to-date effective charge parameterizations are employed, and straggling of ion energy loss is described in "normal" first Born approximation with inclusion of charge exchange effects.

The precise determination of ion range and ionization losses is of utmost importance in dosimetry and in therapeutical applications. For this reason, FLUKA is being heavily benchmarked [37] against models and experimental data concerning ions beams of interest for hadrotherapy. In fig.1 an example of very nice agreement between Bragg peak calculations and data is shown. The contribution of fragmented ions is also evident after the peak.
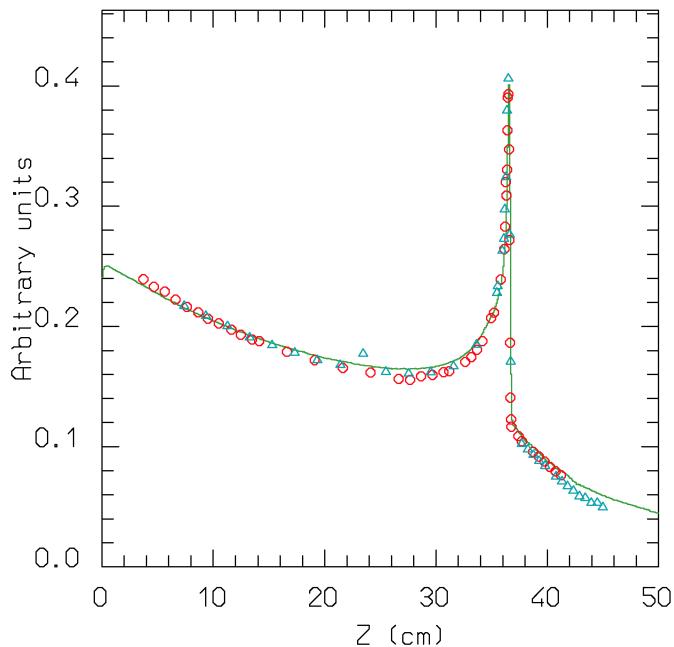
FIGURE 1. Dose versus depth distribution for 670 MeV/n ^{20}Ne ions on a water phantom. The symbols represent LBL (circles) and GSI (triangles) experimental data [38], the line is the prediction of FLUKA including the new BME interface. For the profile reproduction at large depths, nuclear interactions below 100 MeV/n play an important role.

FLUKA HADRONIC MODELS

A basic description of hadronic interactions in FLUKA and of their most recent developments can be found in [14, 15, 16]. Hadron-nucleon interactions at energies below a few GeV are simulated in FLUKA by the isobar model, through resonance production and decay, and by taking into account elastic, charge and strangeness exchange. Elementary hadron-hadron collisions at energies above a few GeV are described thanks to an implementation of the Dual Parton Model (DPM) [17], coupled to a hadronization scheme. This model allows a successful description of soft collision processes that cannot be addressed by perturbative QCD.

Hadron-hadron collisions are the main building blocks of hadron-nucleus collisions. Multiple collisions of each hadron with the nuclear constituents are taken into account by means of the Glauber-Gribov calculus [18, 19]. Particular efforts are devoted to the study of nuclear effects on hadron propagation. These are treated by the FLUKA nuclear interaction model called PEANUT [25, 26, 14, 16]. This model includes a Generalized IntraNuclear Cascade (GINC) with smooth transition to a pre-equilibrium stage performed with standard assumptions on exciton number or excitation energy.

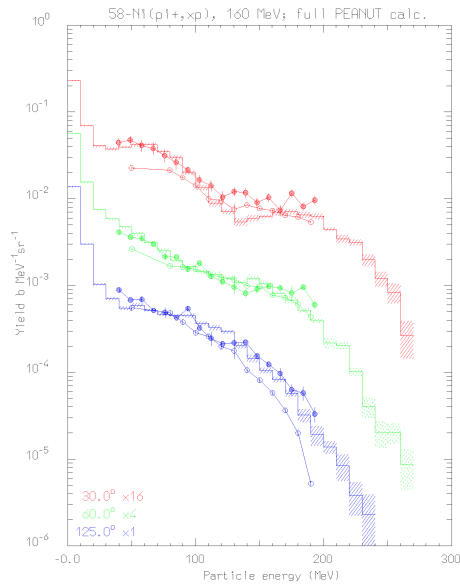GINC modeling in PEANUT is highly sophisticated. Different nuclear densities are

33

FIGURE 2. Emitted proton spectra at different angles, from 160 MeV π^+ on a nickel target. Histograms are FLUKA results, points are experimental data from [28, 29]. Note that proton spectra extend up to 300 MeV
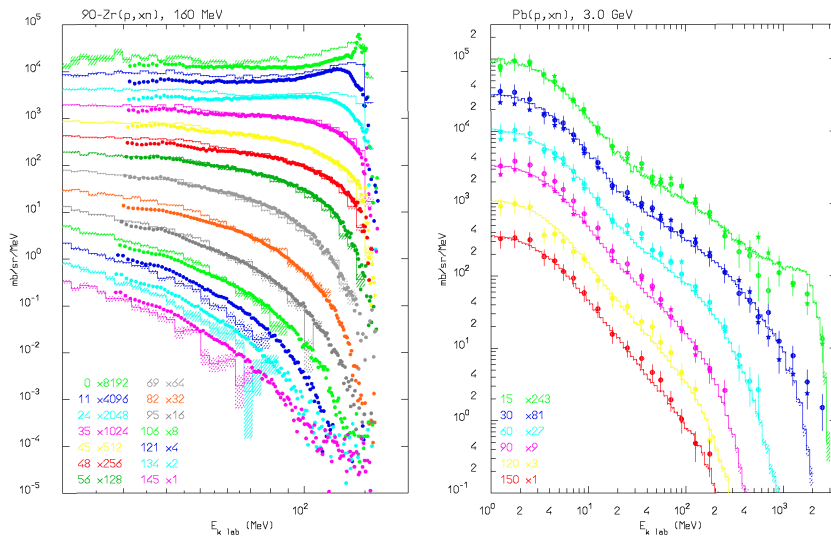

FIGURE 3. Emitted neutron spectra at different angles, from 160 MeV protons on Zr (left) and 3 GeV protons on Pb (right). Histograms are FLUKA results, points are experimental data from [30, 31].

34

adopted for neutrons and protons, Fermi motion is defined locally including wave packet-like uncertainty smearing, the curvature of particle trajectories due to the nuclear potential is taken into account, binding energies are obtained from mass tables and updated after each particle emission, energy-momentum conservation including the recoil of the residual nucleus is ensured. Quantum effects are explicitly included: Pauli blocking, formation zone, nucleon anti-symmetrization, nucleon-nucleon hard-core correlations, coherence length. Nuclear medium effects on the Δ resonance properties are accounted for when treating pion interactions[14, 26] and pion reinteractions in the nucleus (see fig.2 for an example)

The GINC step goes on until all nucleons are below a smooth threshold around 50 MeV, *and* all particles but nucleons (typically pions) have been emitted or absorbed. At the end of the GINC stage a few particles may have been emitted and the input configuration for the pre-equilibrium stage is characterized by the total number of protons and neutrons, by the number of particle-like excitons (nucleons excited above the Fermi level), and of hole-like excitons (holes created in the Fermi sea by the INC interactions), by the nucleus excitation energy and momentum. All the above quantities can be derived by proper counting of what occurred during the INC stage. The exciton formalism of FLUKA follows that of M. Blann and coworkers[20, 21, 22, 23], with some modifications:

- Inverse cross sections from systematics
- Correlation/formation zone/hardcore effects on reinteractions
- Constrained exciton state densities for the configurations 1p-1h, 2p-1h, 1p-2h, 2p-2h, 3p-1h and 3p-2h
- Energy dependent form for the single particle density g_x [24]
- Starting values for the position dependent parameters given by the point like ones as obtained out of the GINC stage.
- Angular distributions of emitted particles in the fast particle approximation

For further details see ref.[14].

PEANUT has proved to be a precise and reliable tool for intermediate energy hadron-nucleus reactions. Its "nuclear environment" is also used in the modelization of (real and virtual) photonuclear reactions, neutrino interactions, nucleon decays, muon captures.

Examples of PEANUT results on neutron production from low energy proton interactions are shown in fig.3. These benchmarks are of high relevance for, for instance, calorimetry. Indeed, even in showers initiated by high energy projectiles, most of the interactions occur at medium-low energies, and the amount of visible energy depends critically on the energy balance and neutron balance in low energy reactions.

Emission of energetic light fragments through the coalescence process is included all along the PEANUT reaction chain. This allows to reproduce the high energy tail of the light fragment spectra, as in fig.4

A major improvement carried out in the last months has been the extension of PEANUT to cover the whole energy range, replacing the simplified intranuclear cascade model that was used for projectile energies larger than 5 GeV. Results obtained with the latest FLUKA version are shown in figs.5, 6 and 7
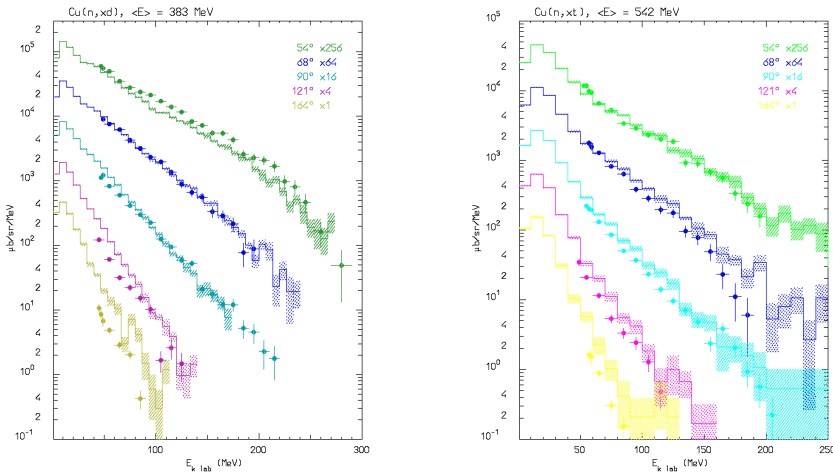
FIGURE 4. Deuteron (left) and triton (right) emission from 383 MeV and 542 MeV neutrons on Cu. respectively (exp data from [27])
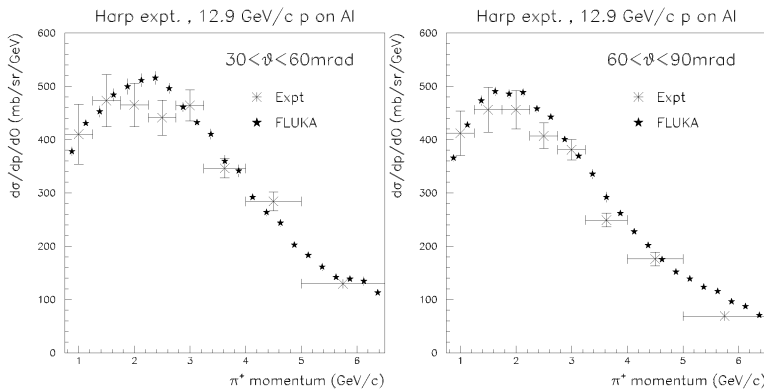

FIGURE 5. Computed π^+ double differential production cross section for 12.9 GeV/c protons on Aluminum for different angular ranges, compared with experimental data [32].

The final steps of the reaction include evaporation in competition with fission and gamma deexcitation. For light nuclei, a Fermi break-up model is implemented. These equilibrium processes are critical for a correct calculation of residual nuclei distributions. This topic is obviously important for activation and residual dose rate studies,it is also indirectly important for calorimetry: since the energy spent in breaking nuclear bonds is a major source of non-compensation and spread in energy deposition, a correct reproduction of residual nuclei distribution is a proof that binding energy losses are correctly taken into account. The FLUKA evaporation model, which is based on the Weisskopf-Ewing approach, has been continuously updated along the years, with the inclusion, for instance, of sub-barrier emission, full level density formula, analytic so-
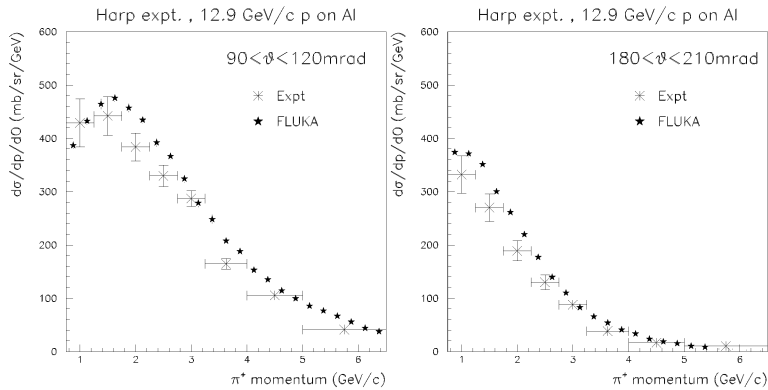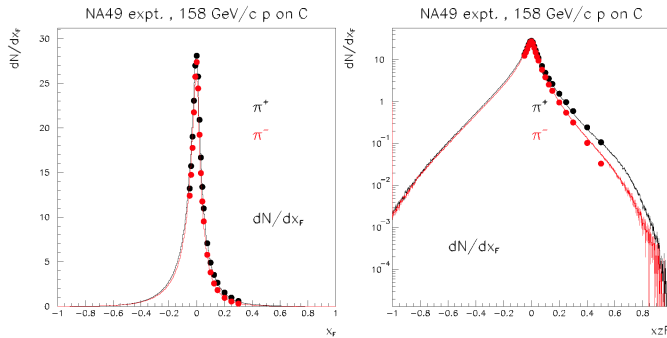
36

FIGURE 6. As fig.5

FIGURE 7. Feynman$-x$ distributions for π^+ and π^- production for proton interactions on Carbon at 158 GeV/c , as measured by NA49 [39] (symbols) and predicted by FLUKA (histograms). Linear scale on the left, logarithmic scale on the right.

lution of the emission widths, evaporation of nuclear fragments up to $A \leq 24$. Recent improvements in the treatment of fission and in the adopted level densities were particularly effective for the description of residual nuclei production from heavy targets. An example of the present code capabilities is shown in fig.8. More complex benchmarks have been carried out at the CERF[41] facility at CERN. Samples of different materials have been irradiated with a mixed hadron field with broad energy spectrum. Comparison of activation and dose rate curves with FLUKA simulations [42] show very nice agreement, as for example in fig9.

LOW ENERGY NEUTRONS

Transport of neutrons with energies lower than 19.6 MeV is performed in FLUKA by a multigroup algorithm. The multi-group technique, widely used in low-energy
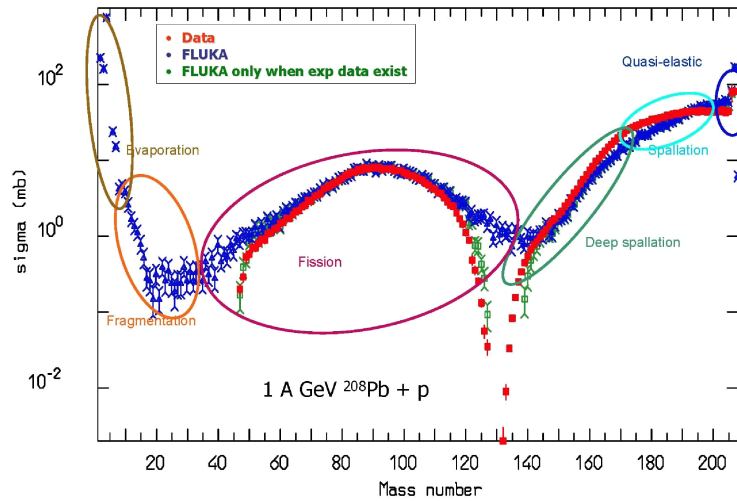
37

FIGURE 8. Residual nuclei production from 1 GeV protons on Lead. Data from [40]
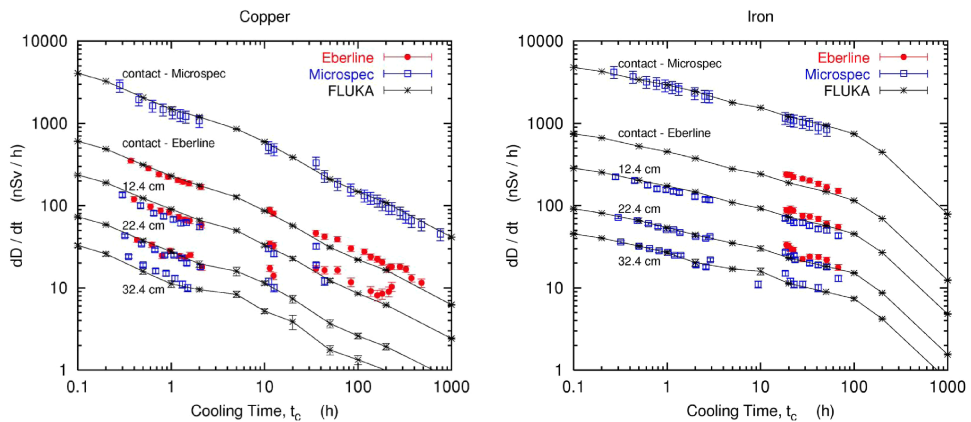

FIGURE 9. Dose rate as a function of cooling time for different distances between sample and detector. Left:Copper sample. Right: iron sample, both irradiated at the CERF facility at CERN. Adapted from [42]

neutron transport programs, consists in dividing the energy range of interest in a given number of intervals ("energy groups"). In the FLUKA cross-section library, the energy range is divided into 72 energy groups of approximately equal logarithmic width (one of which is thermal). The angular probabilities for inelastic scattering are obtained by a discretisation of a P5 Legendre polynomial expansion For a few isotopes only, neutron transport can be done also using continuous (pointwise) cross-sections. For ^{1}H, ^{6}Li and ^{10}B, it is applied as a user option (above 10 keV in ^{1}H, for all reactions in ^{6}Li, and only for the reaction ^{10}B(n,tγ)^{4}He in ^{10}B). For the reaction ^{14}N(n,p)^{14}C,

pointwise neutron transport is always applied. In general, gamma generation by low-energy neutrons (*but not gamma transport*) is treated in the frame of a multigroup scheme too. A downscattering matrix provides the probability, for a neutron in a given energy group, to generate a photon in each of 22 gamma energy groups, covering the range 10 keV to 20 MeV. In all cases, the generated gammas are transported in the same way as all other photons in FLUKA.

NUCLEUS-NUCLEUS INTERACTIONS

Nucleus-nucleus interactions up to 10000 TeV/n are performed through interfaces with external generators. The interface with a modified version of rQMD-2.4 [34, 43] is used for energies below 5 GeV/n. The DPMJET-III [33] code is used from this energy up to the maximum supported one. It is worth mentioning that the external generators, as well as the ones under development, share the same evaporation/deexcitation stage developed for hadron-nucleus interactions. Examples of results can be found in [43, 44]

Work is in progress to complement and eventually substitute the rQMD interface with new QMD codes developed by the FLUKA collaboration[35]. A non-relativistic QMD model has already been interfaced to FLUKA and tests on thin and thick target data are in progress.

The implementation of a Boltzmann Master Equation (BME)[36] model for very low energies is in progress.

GEOMETRY

Transport in arbitrarily complex geometries, including magnetic field, can be accomplished using the FLUKA combinatorial geometry. A suitable voxel geometry module allows to model properly CT scans or other detailed 3D representations of human beings, typically for dosimetry or therapy planning purposes.

FLUGG : the GEANT4 geometry Interface

FLUGG[45] (FLUKA with GEANT4 Geometry) is an extension of FLUKA that uses the GEANT4 geometry package to build the geometry, find the particle locations and boundary interceptions. It provides a more flexible geometry than the default one and allows to run FLUKA using geometry inputs in the GEANT4 format. It has been tested on HP and Linux platforms for single level and multi-level geometries, for neutral and charged particles, including biasing options and magnetic field. An input user interface has been developed, while the output is in FLUKA format.

APPLICATION TO CALORIMETERS

The use of calorimeter data as a benchmark for Monte Carlo codes is a common bad habit. Calorimeters are complex objects, where many physical and instrumental effects are deeply entangled, and can easily mask the goodness or deficiencies of simulation models. Indeed, benchmarking and optimization of codes should be performed on clean data, like thin target or more complex benchmarks in controlled conditions. In this way, codes can then be used to optimize calorimeters design and understand their response. Of course, this does not prevent investigation on the Monte Carlo side in case of disagreement!

FLUKA has been used to simulate calorimeter response, in the framework of the ATLAS and ICARUS collaborations. A few examples and discussion are given in the following subsections.
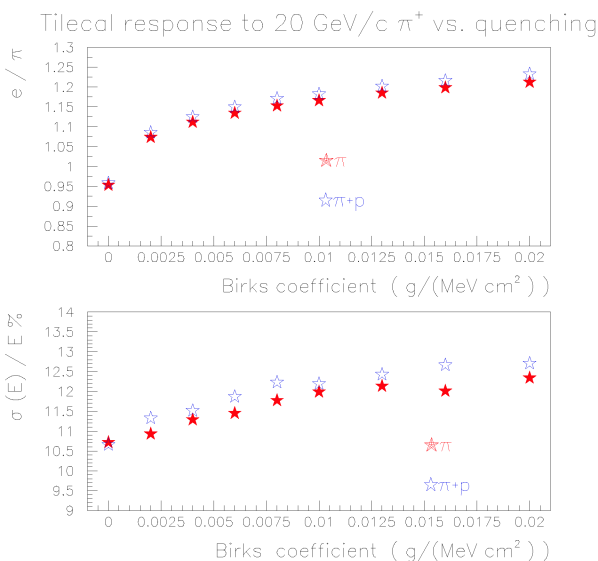
The ATLAS tile calorimeter

FIGURE 10. e/π response (top) and fractional energy resolution (bottom) of the tile calorimeter as a function of the Birks quenching parameter. Simulations for 20 GeV/c π^+ (full red stars) and 20 GeV/c mixed π^+ + proton beam (empty blue stars), at 20° incidence angle.

The ATLAS hadronic calorimeter is composed of scintillator tiles in an iron structure. Several test beams were carried over in the SPS secondary beam lines before the production of the final modules. The results reported here refer to the 1994 setup of the test modules, as reported in [46]. An ensemble of 5 modules was exposed to positron and positive pion beams, with momentum varying from 20 to 300 GeV/c at various angles of incidence. Simulations performed here refer to 20° incidence. The calorimeter geome-
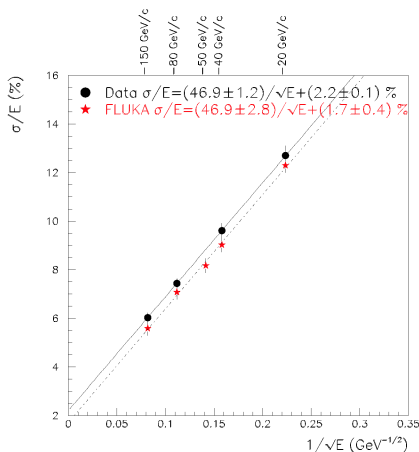
FIGURE 11. Fractional energy resolution as a function of beam energy, for a π^++proton beam at $20°$. Experimental data (dots) from [46].
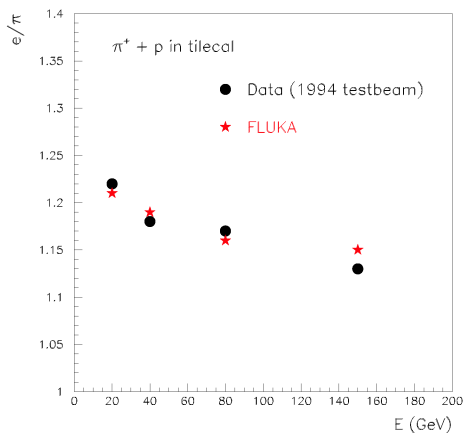

FIGURE 12. As in fig 11 for the relative response to electrons and hadrons.

try was faithfully reproduced, and instrumental effects were included in the calculation. Namely, photostatistics has been convoluted offline as well as random cell-to-cell miscalibration. Signal quenching in scintillator has been simulated on line at each energy deposition. The effect of signal quenching, being proportional to the specific energy loss, is to suppress the signal from slow hadrons and heavy particles. Therefore, it has a strong influence on compensation and energy resolution. As shown in figure10, the iron-scintillator combination would be even over-compensating in the absence of signal quenching, due to neutrons produced in the iron layers and scattering on hydrogen. The e/π signal ratio can vary of more than 10% when the quenching parameter is varied over a "reasonable" range of values. Variations of the same order affect the fractional energy
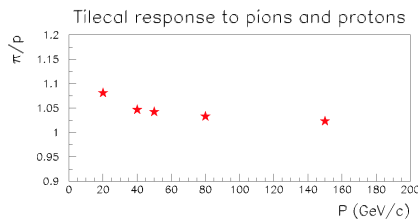
41

FIGURE 13. Simulated relative response to π^+ and protons of the tile calorimeter, as a function of energy. Beam at $20°$ incidence, tile configuration as in [46]

resolution. In the following, a value of $1.30 \cdot 10^{-2}$ $(MeV/(g/cm^2))^{-1}$ has been adopted for the Birks parameter. Simulations also included the proton contamination present in the positive pion beam. This contamination has been both evaluated by FLUKA simulations, and measured with Cerenkov counters during a later test beam[47]. The effect of the proton contamination for the 20 GeV beam is also shown in fig.10 for the 20 GeV/c beam. The effect on resolution is more than 6% for the adopted quenching parameter. The final results of simulations for energy resolution and e/π ratio are shown in figs.11 and 12. A very nice agreement with data is visible.

In pure beams, the simulated response to pions is higher than that to protons, as measured experimentally (see [47] with a different tile configuration) and decreases with energy (see fig.13). Energy resolution is worse for pions (about 10% higher) than for protons, also in agreement with [47].

The ATLAS electromagnetic calorimeter

The ATLAS electromagnetic (E.M.) calorimeter is a lead-liquid argon ionization chamber, with electrodes and absorbers shaped in accordion. Its performances were studied in many test-beams[48]. Comparisons of the response of the E.M. calorimeter to electrons and positrons with FLUKA simulations are very good, both for what concerns energy resolution and shower shape. The calculated energy resolution is $\frac{\sigma_{FLUKA}}{E} = \frac{9.2 \pm 0.3\%}{\sqrt{E}}$, vs an experimental one $\frac{\sigma_{Exp}}{E} = \frac{9.8 \pm 0.4\%}{\sqrt{E}}$. In fig. 14 the dependence of the calorimeter response to the beam impact position is shown. The azimuthal modulation due to the accordion cell structure is well reproduced.

The ATLAS combined calorimeter test beam

Prototypes of the ATLAS electromagnetic and hadronic calorimeters were tested together in 1994 and 1996 with pion beams. The experimental set-up is described in [49, 50], as well as comparisons with simulations. Simulated data were analyzed exactly in the same way as the experimental one, after event-by-event convolution of electronic noise. Calibration was done on an absolute scale. Results for e/π ratios and longitudinal
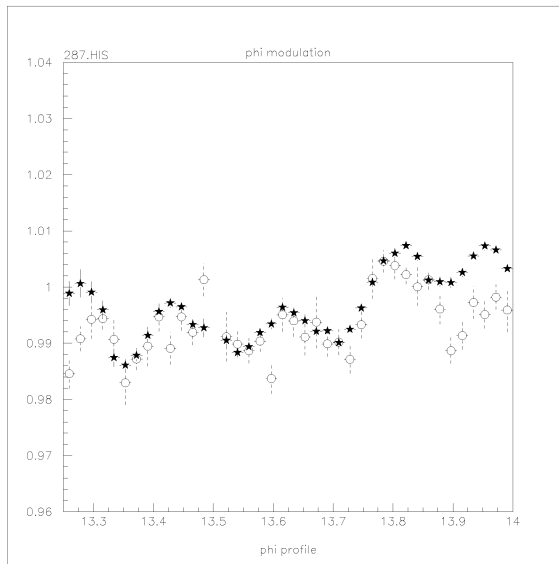
42

FIGURE 14. Modulation of the response of the accordion E.M. calorimeter to a 287 GeV electron beam, as a function of beam impact position. Stars are FLUKA simulations, dots are experimental data. Abscissa values are in ϕ cell units, one cell spanning about 2.5 cm
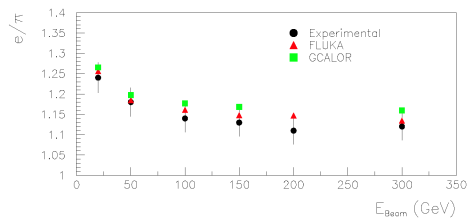

FIGURE 15. Experimental (dots) and simulated (triangles: FLUKA, squares:GCALOR) relative response to electrons and hadrons of the ATLAS combined calorimeter test beam, as a function of beam momentum (adapted from [49])

shower development are reproduced in figs.15 and fig.16. Energy resolution deserves a few comments, demonstrating that care must be taken in considering instrumental effects. In the 1994 test beam a significant discrepancy between measured and simulated energy resolution at 20 GeV/c was found (see fig.17). However, this discrepancy had nothing to do with the physics model used in the simulations, rather it was due to the incomplete knowledge of the beam line characteristics. Indeed, in the 1996 test beam, where the amount of dead materials upstream the detectors was better controlled, the resolution at 20 GeV/c was better and came very near to the simulated value.

In fig.17 two sets of simulation results are presented. The two sets differ only for the details of the algorithm chosen for the reconstruction of the preshower detector response. This detector, a thin lead-liquid argon layer in front of the E.M. calorimeter, was used
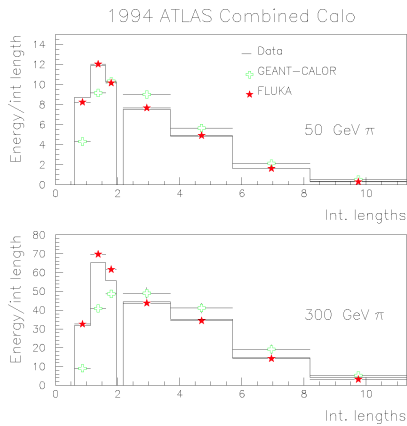
43

FIGURE 16. Longitudinal shower development in the ATLAS combined calorimeter set-up, for 100 GeV/c (top) and 300 GeV/c (bottom) pions. Adapted from [49]
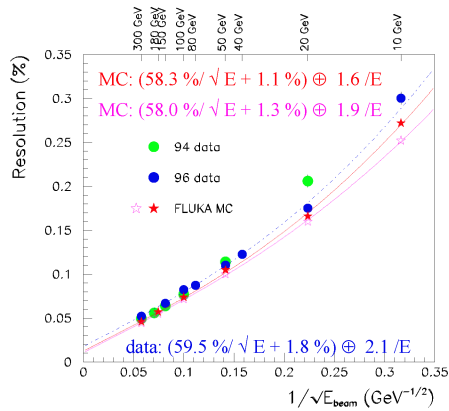

FIGURE 17. Fractional energy resolution as a function of beam momentum for the ATLAS combined calorimeter set-up. Two data sets (dots) correspond to two data takings[49, 50]. Stars: FLUKA simulations with two different preshower reconstruction algorithms.

to veto events with interactions upstream the detector. It is evident that the resolution at low beam energies is heavily affected by the presence of "dirty" events.

44

COSMIC RAY SHOWERS

The application of FLUKA to simulations of cosmic rays showers in the atmosphere began may years ago, with the initial aim to calculate atmospheric neutrino fluxes[56, 57, 58, 59]. This implied the development of more tools, namely:

- Primary spectra from Z = 1 to Z = 28 derived from NASA and updated to most recent measurements (the results of AMS [51] and BESS [52] for proton and helium) and modulated for a given date, according to solar modulation.
- A spherical representation of the earth geometry with the surrounding atmosphere up to 70 km a.s.l.
- The MSIS (Mass-Spectrometer-Incoherent-Scatter) [54] atmospheric model. The atmosphere is layered in 100 shells with a density scaling according to the chosen profile as a function of height.
- A solar modulation model as taken from [53].
- A geomagnetic model, whose degree of complexity can be varied, according to the difficulty of the problem, from a simple dipolar approximation to the spherical harmonic expansion of IGRF[55].

The first important result was that a full 3-dimensional simulation of neutrino fluxes[57] proves to be significantly different from the customary mono-dimensional approximation.

Data on different shower components have been used to benchmark the code[60, 61, 62]. Among the latest calculations[63], we show in fig18 comparisons with experimental muon fluxes at Mount Norikura ($\sim$2700 m a.s.l., 740g/cm^2, 11.2 GV) and at CERN.
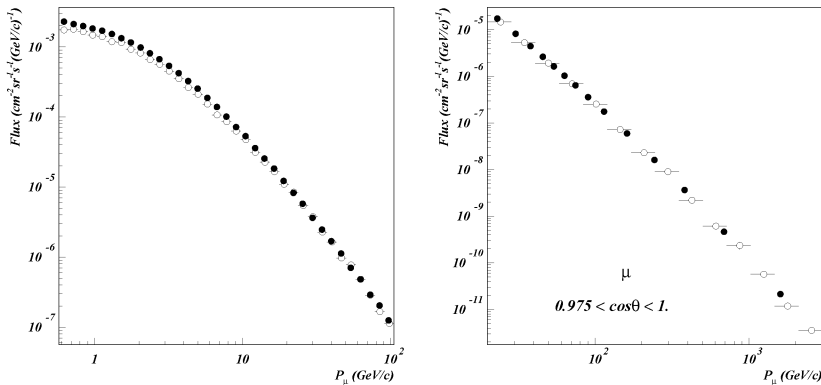

FIGURE 18. left: comparison of the simulated μ^- flux (open symbols) with the BESS[64] experimental data (full symbols) at Mt. Norikura (2700 m a.s.l.). Right: the comparison of simulated $\mu^\pm$ flux at sea level (open symbols) with the L3+C[65] experimental data ($0.975 < cos\theta_z < 1$, full symbols).

Reliable simulations of particle fluxes in the atmosphere are also needed for the evaluation of dose rates on aircrafts. Comparisons of FLUKA prediction with measured doses on commercial aircrafts can be found in [66, 67]. As an example, fig.19 shows the dose equivalent rate on two different aircraft routes. The striking difference between
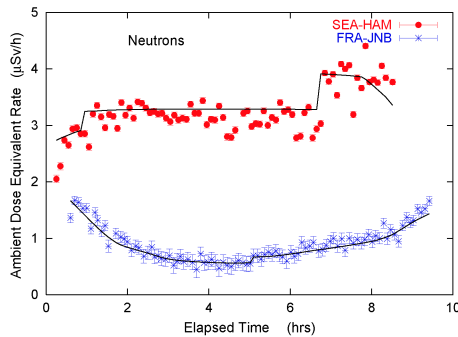
45

FIGURE 19. Ambient dose equivalent from neutrons measured during solar maximum on commercial flights from Seattle to Hamburg and from Frankfurt to Johannesburg, as function of time after take-off (symbols, exp. data, Lines: FLUKA).

polar and equatorial routes is evident, as well as the agreement between simulations and measurements.

NEUTRINO BEAMS AND INTERACTIONS

Many of the improvements to the hadronization model described in [15] were aimed to a better description of hadron production in the CERN Neutrino to GranSasso (CNGS) beam. All simulations for the CNGS facility, from energy deposition to neutrino spectra, are performed with an integrated simulation set-up based on FLUKA[68, 69].

Neutrino interactions are simulated in the framework of the PEANUT nuclear model. Quasi-elastic interactions are generated directly by FLUKA, while for DIS interactions the neutrino-nucleon generator NUX[70] has been interfaced. Work is in progress to develop an internal generator for DIS and resonant reactions.

Nuclear effects on Quasi-Elastic interactions has been tested by comparison with data from the ICARUS 50l prototype exposed to the CERN WANF neutrino beam[71]. In the analysis, "golden" events were selected, i.e. events with only one muon and one identified proton. The input spectrum for the FLUKA event simulation was the one calculated for the NOMAD experiment[72], normalized to the integrated experimental beam intensity. The expected number of quasi-elastic events resulted to be 400, of which 16% were selected as "golden". A 20% background came from DIS events passing the "golden" cuts. As a total, $80 \pm 9(\text{stat.}) \pm 13(\text{syst.})$ were expected, to be compared with 86 events observed. The effect of the nuclear environment on these events is visible in fig20, where the missing transverse momentum distribution is plotted. Dots are the experimental results, the various histograms correspond to simulated quantities. The dashed histogram shows the expected p_{Tmiss} distribution when only the Fermi motion of the target nucleons is taken into account. The distribution is broadened and acquires a high p_{Tmiss} tail when reinteractions inside the nucleus are correctly simulated (dotted histogram), and the agreement with data is further improved when the misidentified (hatched) DIS events are added, summing up to the full response (full line histo). It

46

should be pointed out that the ability to preserve correlations among interaction products is an essential feature in order to reproduce the experimental selection cuts. This is one of the many examples where microscopic models cannot be substituted by data parametrizations.
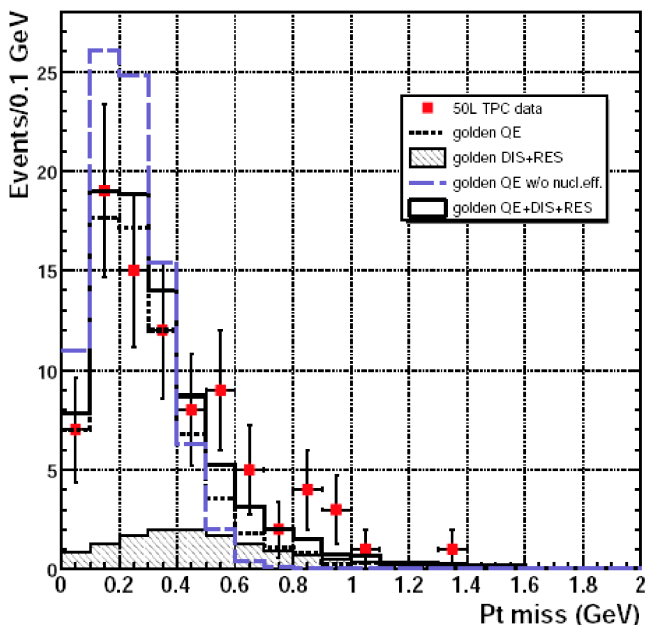

FIGURE 20. p_{Tmiss} distribution of experimental and simulated events in the ICARUS 50l prototype (from [71]). See text.

CONCLUSIONS

FLUKA is a multiparticle transport and interaction Monte Carlo code, able to work both in analog and biased mode. Its physical models are continuously upgraded and benchmarked against experimental data. It has a wide range of applications, in particle physics but also in accelerator design and shielding, dosimetry, radiation protection, hadrotherapy. In particular, it has proven capabilities in the simulation of calorimeters and neutrino beams.

ACKNOWLEDGMENTS

47

REFERENCES

1. A. Ferrari, P.R. Sala, A. Fassò and J. Ranft, CERN 2005-10 (2005), INFN/TC_05/11, SLAC-R-773; A. Fassò et al., Computing in High Energy and Nuclear Physics 2003 Conference (CHEP2003), La Jolla, CA, USA, March 24-28, 2003, (paper MOMT005) eConf C0303241 (2003), arXiv:hep-ph/0306267.
2. A. Fassò, A. Ferrari, J. Ranft, and P.R. Sala, " Proc. of the IV Int. Conf. on Calorimetry in High Energy Physics", La Biodola, (Elba), A. Menzione and A. Scribano eds., World Scientific, p. 493 (1994).
3. R. Brun et al., "GEANT3", CERN DD/EE/84-1 (1987).
4. R.E. Prael and H. Lichtenstein, Los Alamos report **LA–UR–89–3014** (1989)
5. J. Hendricks et al., Los Alamos report **LA-UR-05-2675** (2005).
6. D. Heck et al., Forschungszentrum Karlsruhe Report FZKA 6019 (1998). `http://www-ik.fzk.de/corsika/Welcome.html`
7. D. Heck et al.Forschungszentrum Karlsruhe Report FZKA-6890ZC, Prepared for *28th International Cosmic Ray Conferences (ICRC 2003), Tsukuba, Japan, 31 Jul - 7 Aug 2003*
8. A. Fassò, A. Ferrari, and P.R. Sala, *Proceedings of the MonteCarlo 2000 Conference* A. Kling, F. Barão, M. Nakagawa, L. Távora, P. Vaz eds., Springer-Verlag Berlin, 159 (2001).
9. D.E. Cullen et al.,"EPDL97: the Evaluated Photon Data Library, '97 Version", UCRL–50400, Vol. 6, Rev. 5, 1997.
10. M. Antonelli *et al.*, *Proc. VI Int. Conf. on Calorimetry in High Energy Physics (Calor 96)*, Frascati Physics Series Vol. VI (1997), pp. 561-570
11. G. Battistoni et al., *Nucl. Instr. Meth.* **A394** , 136–145 (1997)
12. A. Ferrari et al., *Nuclear Instr. Meth.* **B71**, 412-426 (1992).
13. A. Fassò et al.in *Proceedings of SARE-3*, H. Hirayama ed., KEK report Proceedings 97-5, 32 (1997).
14. A. Ferrari, and P.R. Sala, *Proceedings of Workshop on Nuclear Reaction Data and Nuclear Reactors Physics, Design and Safety*, A. Gandini, G. Reffo eds., **2**, 424 (1998).
15. G. Collazuol, A. Ferrari, A. Guglielmi, P.R. Sala, *Nucl. Instr. Meth.* **A449**, 609 (2000).
16. G. Battistoni F. Cerutti, A. Ferrari et al., *Proc. 11th Int. Conf. on Nuclear Reaction Mechanisms*, Ric. Scient. ed Ed. Perm. Suppl. , E. Gadioli ed., **126**, 483 (2006).
17. A. Capella, U. Sukhatme, C.-I. Tan and J. Tran Thanh Van, *Phys. Rep* **236**, 225 (1994).
18. R.J. Glauber and G. Matthiae, *Nucl. Phys.* **B21**, 135 (1970).
19. V.N. Gribov, *Sov. Phys. JETP* **29**, 483 (1969).
20. M. Blann, *Phys. Rev. Lett.*, **27**, 337 (1971).
21. M. Blann, *Phys. Rev. Lett.*, **28**, 757 (1972).
22. M. Blann and H.K. Vonach, *Phys. Rev.* **C28**, 1475 (1983).
23. M. Blann, *Phys. Rev.* **C28**, 1648 (1983).
24. S. Shlomo, *Nucl. Phys.* **A539**, 17 (1992).
25. A. Ferrari and P. R. Sala, *Proc. MC93 Int. Conf. on Monte-Carlo Simulation in High-Energy and Nuclear Physics*, World Scientific ed., 277 (1994).
26. A. Fassò, A. Ferrari, J. Ranft, and P. R. Sala, *Proceedings of the "Specialists' Meeting on Shielding Aspects of Accelerators, Targets & Irradiation Facilities"*, p. 287-304 (1995).
27. J. Franz, P. Koncz, E. Rössle, *Nucl. Phys.* **A510**, 774 (1990).
28. Burger et al., *Phys. Rev.* **C41**, 2215 (1990)
29. McKeown et al., *Phys. Rev.* **C24**, 211 (1981)
30. Scobel et al., *Phys. Rev.* **C41** , 2010 (1990);
31. Ishibashi et al., *Nucl. Sci. Technol.* **32**, 827 (1995).
32. The HARP Collaboration, *Nucl. Phys.* **B732**, 1 (2006).
33. S. Roesler, R. Engel and J. Ranft, *Proceedings of the MonteCarlo 2000 Conference*, , A. Kling, F. Barão, M. Nakagawa, L. Távora, P. Vaz eds., Springer-Verlag Berlin, 1033 (2001).
34. H. Sorge, H. Stöcker, and W. Greiner, *Nucl. Phys.* **A498**, 567c (1989).
35. M.V. Garzelli et al., (2005) *Journ. of Phys. : Conference Series* **41** , 519 (2006)
36. F. Cerutti et al., *Journ. of Phys. : Conference Series* **41** , 212 (2006)
37. F. Sommerer, et al.*Physics in Medicine and Biology* **51**, 4385 (2006)
38. L. Sihver et al., *Jpn. J. Med. Phys.* **18**, 1 (1998).
39. C. Alt *et al.*, arXiv:hep-ex/0606028

40. T. Enqvist et al., *Nucl. Phys.* **A 686** 481 (2001).
41. C. Birattari et al., *Radiat. Prot. Dosim.* **76**, 135 (1988)
42. M. Brugger et al., *Radiat. Prot. Dosim.* **116**, 12-15 (2005).
43. V. Andersen et al., *Adv. Space Res.* **34**, 1302 (2004)
44. H. Aiginger, et al., *Adv. Space Res.* **35**, 214-222 (2005)
45. M. Campanella et al., ATL-SOFT-98-039 (1998), ATL-SOFT-99-004 (1999).
46. F. Ariztizabal et al., *Nucl. Instr. Meth.* **349**, 384 (1994)
47. CERN internal note ATL-TILECAL-2001-005
48. D.M. Gingrich et al., *Nucl. Instr. Meth. A364*, 290 (1995)
49. Z. Ajaltouni et al. *Nucl. Instr. Meth.* **A 387**, 333 (1997)
50. S. Akhmadaliev et al,*Nuclear Instruments & Methods A*, **449**, 461-477 (2000).
51. J. Alcaraz et al., *Phys. Lett.* **B490** (2000) 27; J. Alcaraz et al., *Phys. Lett.* **B494** (2000) 193.
52. T. Sanuki et al., *Astrophys. J.* **545** (2000) 1135; K. Abe et al., Phys. Lett. **B564** (2003) 8.
53. G.D. Badhwar, P.M. O Neill, *Adv. Space Res.* **17** n. 2 (1996) 7.
54. MSIS-E-00 Atmosphere Model. Available from: `http://nssdc.gsfc.nasa.gov/space/model/models/msis.html`
55. see `http://swdcwww.kugi.kyoto-u.ac.jp/igrf/index.html`
56. G. Battistoni et al.,*Nucl. Phys. B (Proc. Suppl.)*, **70**, 358 (1998).
57. G. Battistoni et al. ,*Astropart. Phys.*, **12**, 315-333 (2000).
58. G. Battistoni et al.,*Astropart. Phys.* **19**, 269 (2003).
59. G. Battistoni, A. Ferrari, T. Montaruli and P. R. Sala, *Astropart. Phys.* **23** (2005) 526.
60. G. Battistoni, A. Ferrari, T. Montaruli and P. R. Sala, *Astropart. Phys.* **17**, 477-488 (2002).
61. P. Zuccon et al., *Astropart. Phys.* **20**, 221 (2003).
62. S. Muraro, PhD thesis, Milan University (2006)
63. G. Battistoni et al., "Atmospheric muon simulation using the FLUKA MC Model" *proceedings of the NOW06 conference*, in press (2006)
64. T. Sanuki et al. *Physics Letters* **B54**, n. 3-4, (2002) 234;
65. P. Le Coultre, *Proc. of 29th International Cosmic Ray Conference* Pune (2005),00, 101-106 P. Le Coultre and the L3+C collaboration, *Nuclear Physics B - Proc. Supplements*, **151**, n.1 314 (2006).
66. A. Ferrari et al., *Rad. Prot. Dosim.* **93**, 101 (2001) G. Battistoni, A. Ferrari, M. Pelliccioni and R. Villari, *Rad. Prot. Dosim.* **112**, 331-343 (2004); *Adv. Space Res.* **36**, 1645-1652 (2005).
67. S. Roesler, W. Heinrich and H. Schraube, *Radiation Research* 149, 87 (1998); *Radiation Protection Dosimetry* **98**, 367-388 (2002)
68. A. Ferrari et al., CERN-AB-Note-2006-038 (2006).
69. A. Ferrari et al., *CNGS neutrino beam: from CERN to GranSasso*, presented at the NOW06 conference.
70. A. Rubbia "NUX- neutrino generator", *1st Workshop on Neutrino - Nucleus Interactions in the Few GeV Region (NuInt01)*, Tsukuba, Japan, 13-16 Dec 2001, `neutrino.kek.jp/nuint01/slide/Rubbia.1.pdf`
71. F. Arneodo et al.,*Phys. Rev. D 74*, 112001 (2006).
72. P. Astier et al., *Nucl. Instr. and Meth.* **A 515**, 800 (2003).